ACADEMIC PRESS

Available online at www.sciencedirect.com

SCIENCE DIRECT®

Journal of Computational Physics 186 (2003) 582–595

JOURNAL OF COMPUTATIONAL PHYSICS

www.elsevier.com/locate/jcp

# Robust numerical simulation of porosity evolution in chemical vapor infiltration III: three space dimension

Shi Jin [a,*,1], Xuelei Wang [b]

[a] *Department of Mathematics, University of Wisconsin-Madison, Madison, WI 53706, USA*
[b] *School of Mathematics, Georgia Institute of Technology, Atlanta, GA 30332, USA*

Received 19 September 2002; accepted 29 January 2003

**Abstract**

Chemical vapor infiltration (CVI) process is an important technology to fabricate ceramic matrix composites (CMC's). In this paper, a three-dimension numerical model is presented to describe pore microstructure evolution during the CVI process. We extend the two-dimension model proposed in [S. Jin, X.L. Wang, T.L. Starr, J. Mater. Res. 14 (1999) 3829; S. Jin. X.L. Wang, T.L. Starr, X.F. Chen, J. Comp. Phys. 162 (2000) 467], where the fiber surface is modeled as an evolving interface, to the three space dimension. The 3D method keeps all the virtue of the 2D model: robust numerical capturing of topological changes of the interface such as the merging, and fast detection of the inaccessible pores. For models in the kinetic limit, where the moving speed of the interface is constant, some numerical examples are presented to show that this three-dimension model will effectively track the change of porosity, close-off time, location and shape of all pores.


## 1. Introduction

Chemical vapor infiltration (CVI) is an important and widely used technology for fabricating fiber reinforced ceramic matrix composite (CMC's). Numerous types of composites can be fabricated by the CVI [1,2].

In the CVI process of fabricating the carbon/silicon carbide (C/SiC) composite, the preform, which is a porous array of carbon fibers, is placed in a furnace with elevated temperature. A vapor precursor of the matrix material, such as the methyltrichlorosilane (MTS), diffuses through or is forced into the preform. The MTS dissociates at the fiber surface and deposits a layer of solid SiC coating (also called matrix) on the surface, filling the inter-fiber void. As the deposition progress continues, the spaces between the fibers become smaller, and avenues for gas transport become more tortuous and begin to close off, forming

* Corresponding author. Tel.: +1-608-263-3302; fax: +1-608-263-8891.
*E-mail addresses:* jin@math.wisc.edu (S. Jin), xwang@math.gatech.edu (X. Wang).
[1] Research was supported in part by NSF Grant DMS-0196106.

0021-9991/03/$ - see front matter © 2003 Elsevier Science B.V. All rights reserved.
doi:10.1016/S0021-9991(03)00083-4

inaccessible pores and preventing vapor precursor from penetrating further into the the fiber preform. The process of infiltration and deposition eventually ceases as long as the void spaces between fibers no longer form a percolating network through the composites. Under most processing conditions, the transport of vapor precursor from the surroundings is far more rapid than the deposition, and matrix growth continues as long as there is a continuous path from fiber surface to the surrounding source of vapor precursor.

As described above, the volume of the solid phase increases and porosity decreases as the CVI process continues. This may lead to the formation of inaccessible pore space, and more space may become inaccessible to gas transport from outside as the reaction proceeds further. The lowest porosity that permits percolation of a fluid through the pore space is an important characteristic, since it determines the microstructure and other mechanic property of the final composite product. The CVI process also exemplifies a more general physical phenomenon of gas–solid reaction involving porous solids, which is accompanied by increasing volume of solid phase and decreasing porosity of the porous medium due to the formation of solid or deposition of a solid species on the gas–solid interface. So the models for CVI can also be applied to a variety of gas–solid reaction processes.

Since the earliest work on CVI by Bickerdike et al. [18], many mathematical models have been established to study the process, especially after late 1980s. Many aspects of the process have been invested, including reaction and diffusion kinetics, thermal conductivity and gas permeability, porosity changes and pore microstructure evolution, simulation of matrix growth on fibers, etc [21]. Several approaches have been used in these models. One natural way is to use a gas transport-reaction equation and/or an equation of conservation of mass [6,7,15]. Some models are built on the assumption that pores are cylindrical and use the geometry property of a cylinder to achieve an analytical expression for the porosity [8,17]. These are generally one-dimensional models, in which pore microstructure evolution is studied through the change of macroscopic quantities such as porosity. These models are generally not be able to extended to higher dimensions. Most two-dimensional models take the common approach by simulating the cross section of a bundle of fibers by a group of expanding/overlapping circles [9–12]. These models are used to study gas transport properties and thermal conductivity other than pore microstructure changes.

The level set model proposed in [13,14,16] also takes the expanding/overlapping circles approach, but it simulates the pore microstructure evolution in CVI by modeling the gas–solid interface as an evolving front. The level set equation is used to overcome the computational difficulty of capturing the topological changes in pore evolution. A Fast Searching Method, similar to the Fluid-Fill algorithm in computer graphics [5], was also developed to detect inaccessible pores when they have formed. In [14,16] numerical methods are presented for this model in two space dimension, for the kinetic limit and the anisotropic growth rate, respectively.

Even thought there are a plenty of lower dimensional CVI models, the lack of three-dimensional model for pore evolution is still a big hindrance for numerical simulation and theoretical understanding of the CVI process. In reality, the cylindrical fibers in CVI preform are three-dimensional objects, so are the pores and gas transport path. The two-dimensional cross-section model cannot capture the complexity of the three-dimensional geometry.

In this paper, we present the 3D numerical method for CVI by extending our level set model introduced in [13,14] to the three space dimension. As in [14], we assume that the process is in its kinetic limit, where the front speed is constant unless around inaccessible pores. This state can be achieved under optimal processing condition. We also extend the 2D Fast Searching Method for the detection of inaccessible pores into 3D.

This paper is organized as follows. In Section 2, we introduce the three-dimensional model based on our previous work [13,14]. In Section 3, we first present the second order numerical scheme for the three-dimensional *Hamilton–Jacobi* equation by Osher and Sethian [19], and then make the three-dimensional extension of the Fast Searching Method for the detection of inaccessible pores. Two numerical examples are given in Section 4 to test the model and the numerical method. We conclude this paper in Section 5.

## 2. The mathematical model

In [13,14], a model based on the level set equation of the Hamilton–Jacobi type, coupled with a boundary value problem of the Laplace equation, was introduced for the CVI process. This model is valid for any space dimension. In 3D, the fiber fronts are surfaces. Below we review this model.

Assume that the CVI process takes place in a cube (see Fig. 1). We need the following notations to describe the model:

$\Omega$ the cubic region where the fibers are placed and grown,
$\partial\Omega$ the outer boundary of the cubic region,
$\Omega^+$ the space occupied by gas reagent,
$\Omega^-$ the space occupied by developed fibers,
$\Gamma$ the fiber front, i.e., the gas/fiber interface,
$O$ the inaccessible pores where the gas cannot reach from $\partial\Omega$.

Let $\phi(\vec{x},t)$ be the level set function, with zero level set $\Gamma_t = \{\vec{x}|\phi(\vec{x},t) = 0\}$ representing the evolving gas/fiber interface at time $t$. Generally, the initial choice of $\phi$ is the signed distance function, $\phi(\vec{x},t=0) = \pm d$, where $d$ is the distance from point $\vec{x}$ to $\Gamma_0$, the initial fiber surface. The plus (+) or minus (−) sign is chosen if the point $\vec{x}$ is outside (in gas phase) or inside (in solid phase) $\Gamma_0$, respectively. At time $t$, the solid and gas phases are represented by $\Omega^- = \{\vec{x}|\phi(\vec{x},t) < 0\}$ and $\Omega^+ = \{\vec{x}|\phi(\vec{x},t) > 0\}$, respectively.

Let $\alpha(\vec{x},t)$ denote the accessibility of point $\vec{x}$ to gas reagent at time $t$, i.e.

$$\alpha(\vec{x},t) = \begin{cases} 1 & \text{if } \vec{x} \text{ is accessible,} \\ 0 & \text{if } \vec{x} \text{ is inaccessible,} \end{cases} \tag{1}$$

and $c(\vec{x},t)$ be the growth speed of $\Gamma$ in the normal direction. The level set function $\phi$ then solves the following Hamilton–Jacobi equation:

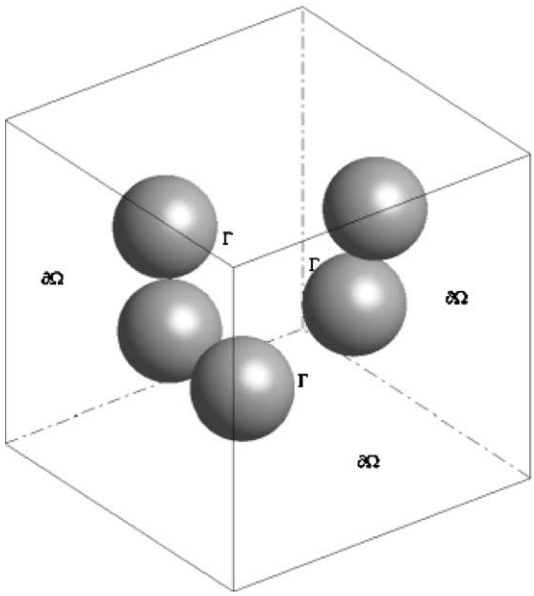


Fig. 1. Model description in 3D.

$$\begin{cases} \frac{\partial\phi(\vec{x},t)}{\partial t} - \alpha(\vec{x},t)c(\vec{x},t)|\nabla\phi(\vec{x},t)| = 0, \\ \phi(\vec{x},t=0) = \pm d. \end{cases} \tag{2}$$

During the front propagating process, inaccessible pores (area $O$) may form, where the gas from $\partial\Omega$ cannot reach, thus the surface surrounding the area will stop growing. A main contribution of this model is to incorporating the accessibility $\alpha(\vec{x},t)$ in the level set Eq. (2) in order to correctly describe the behavior of the inaccessible pores which ceases to grow. The accessibility function $\alpha(\vec{x},t)$ may be determined from another equation satisfied by a concentration variable (or an order parameter) $u(x,t)$, defined in $\Omega^+$ and solving the following boundary value problem of the Laplace equation:

$$\begin{cases} \Delta u(\vec{x},t) = 0, & \text{in } \Omega^+(t), \\ u(\vec{x},t) = 1, & \text{on } \partial\Omega, \\ u(\vec{x},t) = 0, & \text{on } \Gamma_t. \end{cases} \tag{3}$$

By the Maximum Principle [3], the solution of (3) satisfies $0 \leqslant u \leqslant 1$ on $\Omega^+(t)$, and the maximum value 1 and the minimum value 0 are attained only at the boundary $\partial\Omega$ and $\Gamma_t$, respectively. For inaccessible pore area $O$, $u$ defined in $O$ has zero boundary condition on the boundary of $O$, which is part of $\Gamma$, thus the Maximum Principle implies that $u \equiv 0$ in $O$. On the other hand, $0 < u < 1$ in the accessible region. So,

$$\alpha(\vec{x},t) = \begin{cases} 1 & \text{if } u > 0, \\ 0 & \text{if } u = 0 \quad \text{and} \quad \phi > 0. \end{cases} \tag{4}$$

In general the growth speed $c$ depends on $u$. However, in the kinetic limit, in which the growth speed $c$ is a constant, one can avoid solving (4). Instead, the inaccessible pores can be detected by a Fast Searching Method developed in [14]. This algorithm can be easily extended to three space dimension. The details will be given in the following section.

## 3. Numerical methods

### 3.1. Discretization of the Hamilton–Jacobi equation

To solve the Hamilton–Jacobi equation (2), we use the second order scheme introduced by Osher and Sethian [4,19].

Let $D^{\pm}$ denote the finite difference operator

$$D^{\pm x}\phi \equiv \frac{\phi(x \pm h, t) - \phi(x,t)}{\pm h}.$$

Then the numerical scheme for (2) can be described as following:

$$\phi_{ijk}^{n+1} = \phi_{ijk}^{n} + \Delta t[\max(F_{ijk},0)\nabla^+ + \min(F_{ijk},0)\nabla^-], \tag{5}$$

where $F = \alpha(\vec{x},t)c(\vec{x},t)$ is the normal speed of $\Gamma$, $\nabla^+$, $\nabla^-$ are given by

$$\nabla^+ = [\max(A,0)^2 + \min(B,0)^2 + \max(C,0)^2 + \min(D,0)^2 + \max(E,0)^2 + \min(F,0)^2]^{1/2}, \tag{6}$$

$$\nabla^- = [\max(B,0)^2 + \min(A,0)^2 + \max(D,0)^2 + \min(C,0)^2 + \max(F,0)^2 + \min(E,0)^2]^{1/2}, \tag{7}$$

with

$$A = D_{ijk}^{-x} + \frac{\Delta x}{2} m(D_{ijk}^{-x-x}, D_{ijk}^{+x-x}), \tag{8}$$

$$B = D_{ijk}^{+x} - \frac{\Delta x}{2} m(D_{ijk}^{+x+x}, D_{ijk}^{+x-x}), \tag{9}$$

$$C = D_{ijk}^{-y} + \frac{\Delta y}{2} m(D_{ijk}^{-y-y}, D_{ijk}^{+y-y}), \tag{10}$$

$$D = D_{ijk}^{+y} - \frac{\Delta y}{2} m(D_{ijk}^{+y+y}, D_{ijk}^{+y-y}), \tag{11}$$

$$E = D_{ijk}^{-z} + \frac{\Delta y}{2} m(D_{ijk}^{-z-z}, D_{ijk}^{+z-z}), \tag{12}$$

$$F = D_{ijk}^{+z} - \frac{\Delta y}{2} m(D_{ijk}^{+z+z}, D_{ijk}^{+z-z}). \tag{13}$$

The minmod slope limiter function $m(x, y)$ is defined by

$$m(x,y) = \begin{cases} \begin{cases} x & \text{if } |x| \leqslant |y| \\ y & \text{if } |x| > |y| \end{cases} & \text{if } xy \geqslant 0; \\ 0 & \text{if } xy < 0. \end{cases} \tag{14}$$

### 3.2. A fast searching method for detecting the inaccessible pores

An efficient algorithm for detecting inaccessible pores in 2D was developed in [14]. This algorithm can be easily extended to 3D.

Assume a rectangular mesh is used for the computational domain $\Omega$. At time $t$, let $\mathscr{B}$ be the set of points in $\Omega^+$ that are accessible from the boundary $\partial\Omega$. Initially, put the boundary points, where the reactant comes in, into set $\mathscr{B}$. Starting with any point $\vec{x} = (i, j, k)$ in $\mathscr{B}$, put into $\mathscr{B}$ all its nearest neighboring points $\{(i \pm p_i, j \pm p_j, k \pm p_k) | p_i, p_j, p_k = -1, 0, 1 \text{ and } |p_i| + |p_j| + |p_k| > 0\}$ that belong to $\Omega^+$ but not already in $\mathscr{B}$. Then go to the next point in $\mathscr{B}$ and repeat the previous procedure until all points in $\Omega^+$ have been checked. Then $\alpha(\vec{x}, t) = \chi_{\mathscr{B}}(\vec{x})$, the characteristic function of set $\mathscr{B}$.

If we assume the points in set $\mathscr{B}$ are ordered by the order of being added into the set, and use another function $C(i, j, k)$ to indicate whether a point $(i, j, k)$ is checked or not in the process, the algorithm can be described as follows:

1. Initialize $\mathscr{B} = \emptyset$, and $C(i, j, k) = 0$ for all points.
2. Check all boundary points $\{(i, j, k) | i = 0, \text{ or } j = 0, \text{ or } k = 0, \text{ or } i = N, \text{ or } j = N, \text{ or } k = N\}$, if a boundary point $(i, j, k) \in \Omega^+$ (i.e., $\phi(i, j, k) > 0$ ), then put $(i, j, k)$ into $\mathscr{B}$ and set $C(i, j, k) = 1$.
3. Pick up the first point $(i_0, j_0, k_0)$ in $\mathscr{B}$.
4. Repeat: (1) Check all neighboring points of $(i_0, j_0, k_0)$, namely, points $\{(i_0 \pm p_i, j_0 \pm p_j, k_0 \pm p_k) | p_i, p_j, p_k = -1, 0, 1 \text{ and } |p_i| + |p_j| + |p_k| > 0\}$. If a neighboring point $(i, j, k) \in \Omega^+$ (i.e., $\phi(i, j, k) > 0$) and $C(i, j, k) = 0$, then put $(i, j, k)$ into $\mathscr{B}$ and set $C(i, j, k) = 1$. (2) Choose the next point in $\mathscr{B}$, denote it as $(i_0, j_0, k_0)$ and go to (1) until all points in $\mathscr{B}$ have been processed by this procedure.

At each time step, every point at $\Omega^+$ will be moved into $\mathscr{B}$ at most once. Thus this algorithm needs at most $O(N^3)$ operations for each time step, where $N$ is the number of grid points in one axis-direction. In

fact, at the later stage when the residual porosity becomes small, the number of operations is far less than $O(N^3)$ since only the points in $\Omega^+ - O$ are moved into $\mathscr{B}$.

### 3.3. Calculation of the porosity

To calculate the porosity numerically, the simplest method is used. First the total number of cells with $\phi > 0$ are counted, then it is divided by the total number of cells. This is a first order calculation. A second order calculation of porosity will be far more complex than the one used in [14] and will not be used here.

### 3.4. Formation time and graphic display of the inaccessible pores

At each time step, based on the level set function $\phi$ and the accessibility function $\alpha(\vec{x}, t)$, all grid points in the region can be categorized into three types:

$$\vec{x} = (i,j,k) \in \begin{cases} \Omega^- : \phi(\vec{x},t) < 0, \text{ solid phase;} \\ \Omega^+ : \phi(\vec{x},t) > 0 \text{ and } \alpha(\vec{x},t) = 1, \text{ accessible gas phase;} \\ O : \phi(\vec{x},t) > 0 \text{ and } \alpha(\vec{x},t) = 0, \text{ inaccessible pores.} \end{cases}$$

By tracking the change of the size of set $O$—the number of grid points in set $O$, we can easily see when the inaccessible pores form: whenever the size of $O$ increases, there must be at least one inaccessible pore that closes off at that time.

It is not trivial to display the pores in 3D. In 2D, the location of pores can be easily viewed from the plot of the microstructure. When a 3D geometry of the microstructure is plotted in a two-dimension picture (the cross-section), the pores will not be easily seen from the picture. We utilize an algorithm similar to the one in Section 3.2 to detect and group these pores, and then display only these pores graphically. This algorithm has some similarity with the cluster multiple labeling technique [20].

1. Initialize $P(i,j,k) = 0$ for all $i,j,k$.
2. Initialize $L = 0$, set $\Psi = \emptyset$
3. for $i = 0$ to $N$, $j = 0$ to $N$, $k = 0$ to $N$, if $P(i,j,k) = 0$ and $\alpha(i,j,k) = 0$ and $\phi(i,j,k) > 0$ then
   (a) $L = L + 1, P(i,j,k) = L$, add $(i,j,k)$ to set $\Psi$
   (b) Get the first point $(i_0, j_0, k_0)$ in $\Psi$.
   (c) Repeat: (1) Check all neighboring points of $(i_0, j_0, k_0)$, namely, $\Theta = \{(i_0 \pm p_i, j_0 \pm p_j, k_0 \pm p_k)$ $|p_i, p_j, p_k = -1, 0, 1$ and $|p_i| + |p_j| + |p_k| > 0\}$: if $(i_x, j_x, k_x) \in \Theta$ and $P(i_x, j_x, k_x) = 0$ and $\alpha(i_x, j_x, k_x) = 0$ and $\phi(i_x, j_x, k_x) > 0$ then, $P(i_x, j_x, k_x) = L$, put $(i_x, j_x, k_x)$ to set $\Psi$ (2) Take the next point in $\Psi$, denote it as $(i_0, j_0, k_0)$ and go to (1) until all points in $\Psi$ have been processed.

When this algorithm ends, $L$ will be the total number of inaccessible pores, while the pores are grouped by the values of $P(i,j,k)$. Each pore is prescribed into a cubic box. Let $\Sigma_m = \{(i,j,k)|P(i,j,k) = m\}$, $(m = 1, 2, \ldots, L)$ be the $m$th pore. It is bounded by the cubic box

$$[x(i_{\min}), x(i_{\max})] \times [y(j_{\min}), y(j_{\max})] \times [z(k_{\min}), z(k_{\max})]$$

where

$$i_{\min} = \min\{i|(i,j,k) \in \Sigma_m\},$$

$$i_{\max} = \max\{i|(i,j,k) \in \Sigma_m\},$$

and $j_{\min}, j_{\max}, k_{\min}$ and $k_{\max}$ are defined similarly.

## 4. Numerical results

In this section we present some numerical experiments on the 3D pore evolution using the method described in Section 3.

The computation is carried out over an $2 \times 2 \times 2$ cubic region $[-1,1] \times [-1,1] \times [-1,1]$ with periodic boundary condition for $\phi$, and in each space dimension 80 grid points are used, with time step ($\Delta t = 1.25 \times 10^{-2}$) satisfying the numerical stability condition. Three-dimensional balls are used to represent the fibers. And for simplicity, we assume that all fibers grow at a constant speed $c \equiv 1$. During the computation process, we only monitor the unit cube $[-0.5, 0.5] \times [-0.5, 0.5] \times [-0.5, 0.5]$ centered at the computational domain: all balls are initially placed in the central cube without overlapping with each other or with the boundary of the central cube. All pictures are drawn only for the central cube and the porosity is also calculated against the central cube (unless explicitly stated). By doing this we avoid any special treatment needed when the balls hit the boundary of the computational domain.

We test the numerical method for the following three cases: (1) $2^3 = 8$, uniformly distributed in the central cube; (2) $3^3 = 27$ balls uniformly distributed in the central cube; (3) 63 balls randomly distributed in the central cube. In the first two cases, exact solutions are compared with the numerical result.

**Example 1.** Initially we place 8 balls on a cubic lattice. The balls are centered at $(\pm 0.25, \pm 0.25, \pm 0.25)$ respectively, all with the same radius $r = 0.15$ (see Fig. 2).

When the two balls on diagonal lines "touch" each other (hence radius is $0.25\sqrt{2} \approx 0.3535$), the inaccessible pore forms. So the pore forming time $= 0.3535 - 0.15 = 0.2035$. The exact pore size can be calculated as following: in each octant, for example in the first octant, the pore is formed by three coordinate planes and the ball $(x - 0.25)^2 + (y - 0.25)^2 + (z - 0.25)^2 = (0.25\sqrt{2})^2$; the pore volume in one octant is

$$\int_0^{0.25} \int_0^{\sqrt{0.25^2-(x-0.25)^2}} \int_0^{\sqrt{(0.25\sqrt{2})^2-(x-0.25)^2-(y-0.25)^2}} 1 \, dz \, dy \, dx \approx 5.80 \times 10^{-4}.$$

So the volume of whole pore is $8 \times 5.80 \times 10^{-4} \approx 0.0046$.

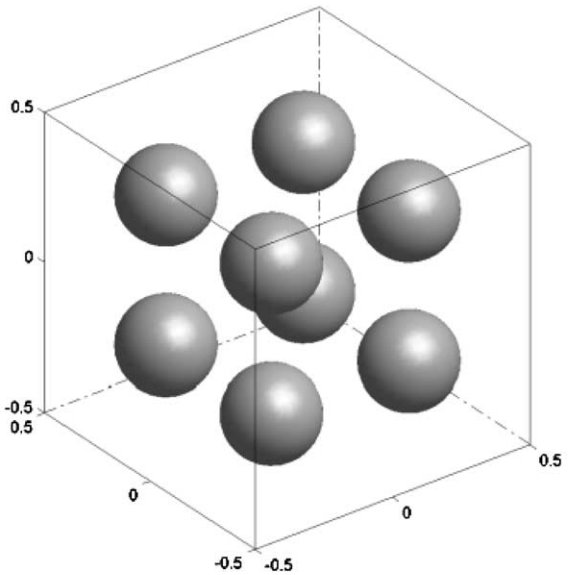


Fig. 2. Initial distribution: 8 balls.

Using the numerical scheme of this model, we calculate the first 24 time steps, and plot the pore size and porosity at each time step (Fig. 4). As Fig. 4(a) indicates, the inaccessible pore or pores form at $t = 16\Delta t = 0.2$, and pore size is 321 grid points (Fig. 4(b)) which corresponds to volume 0.0047.

Using the algorithm described in Section 3.4 for detecting the inaccessible pores, we find one pore contained in cube $[-0.2, 0.2] \times [-0.2, 0.2] \times [-0.2, 0.2]$, as shown in Fig. 3.

**Example 2.** Initially we place 27 balls on the cubic lattice. The balls are centered at ($\pm 0.3$ or 0, $\pm 0.3$ or $0, \pm 0.3$ or 0) respectively, all with the same radius $r = 0.10$ (see Fig. 5).

As in Example 1, the exact time of pore formation is $0.15\sqrt{2} \approx 0.2121 - 0.10 = 0.1121$. Since there are 8 inaccessible pores, the volume of all these pores is

$$8 \times 8 \times \int_0^{0.15} \int_0^{\sqrt{0.15^2-(x-0.15)^2}} \int_0^{\sqrt{(0.15\sqrt{2})^2-(x-0.15)^2-(y-0.15)^2}} 1 \, dz \, dy \, dx \approx 8 \times 8 \times 1.25 \times 10^{-4} \approx 0.0080.$$

For the first 24 time steps of numerical solution, we plot the pore size and porosity at each time step (Fig. 7). As Fig. 7(a) indicates, the inaccessible pore or pores form at $t = 9\Delta t = 0.1125$. Fig. 7(b) shows that the pore size is 552 grid points which corresponds to volume 0.0080.

Using the algorithm of Section 3.4 for detecting the inaccessible pores, we find 8 pores contained in the following cubes, respectively,

1. $[-0.25, -0.05]^3$,
2. $[-0.25, -0.05]^2 \times [0.05, 0.25]$,
3. $[-0.25, -0.05] \times [0.05, 0.25] \times [-0.25, -0.05]$,
4. $[-0.25, -0.05] \times [0.05, 0.25]^2$,
5. $[0.05, 0.25] \times [-0.25, -0.05]^2$,
6. $[0.05, 0.25] \times [-0.25, -0.05] \times [0.05, 0.25]$,
7. $[0.05, 0.25]^2 \times [-0.25, -0.05]$,
8. $[0.05, 0.25]^3$.

These pores are depicted in Fig. 6.

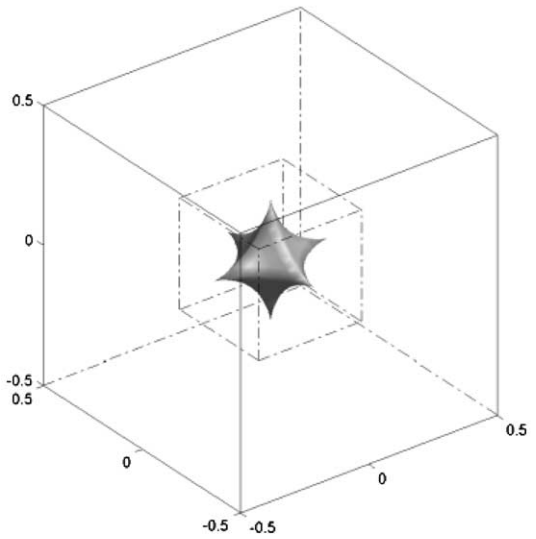


Fig. 3. Inaccessible pore, shape and location: 8 balls.

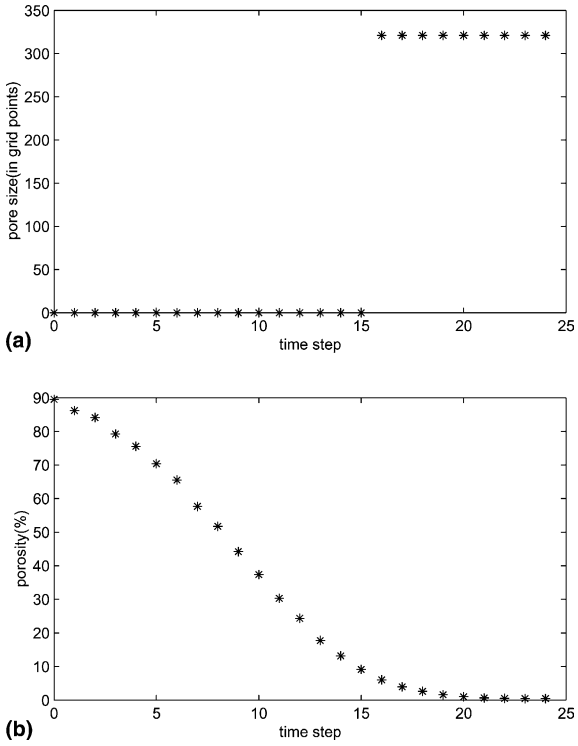


Fig. 4. Pore size and porosity vs. time: 8 balls. (a) Size of inaccessible pore(s) vs. time. (b) Porosity vs. time.

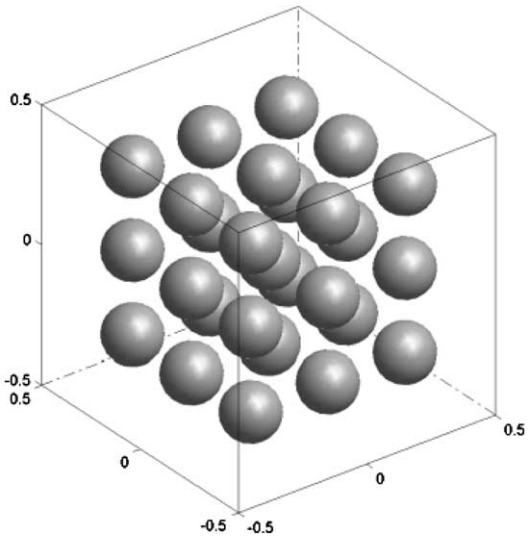

Fig. 5. Initial distribution: 27 balls.

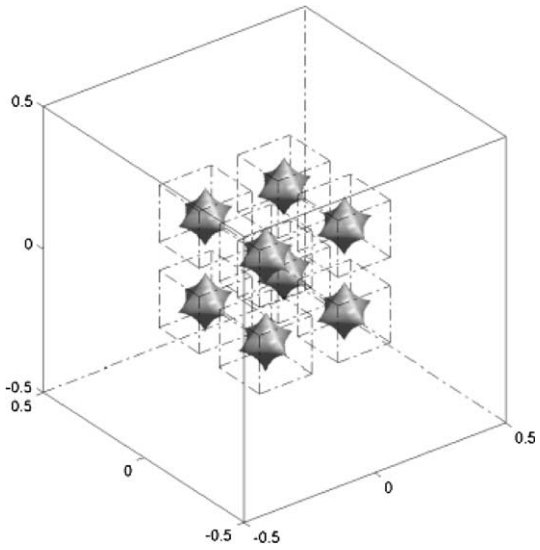


Fig. 6. Inaccessible pore, shape and location: 27 balls.

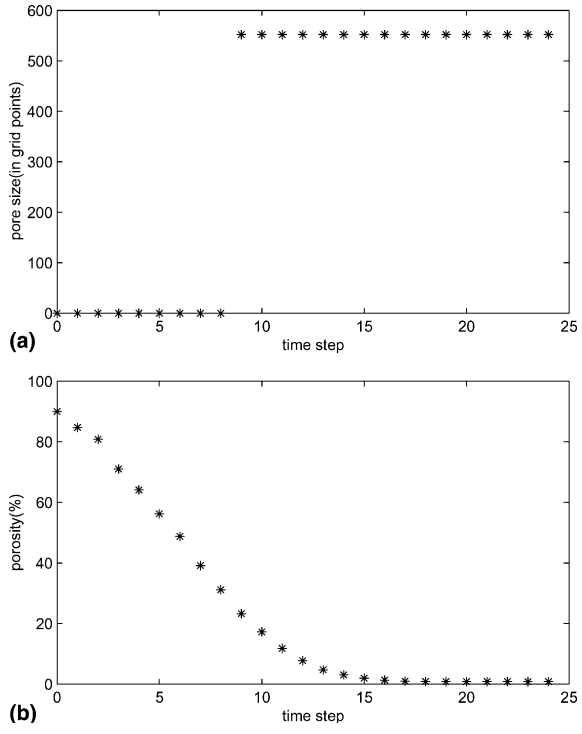


Fig. 7. Pore size and porosity vs time: 27 balls. (a) Size of inaccessible pore(s) vs. time. (b) Porosity vs. time.

**Remark.** In Examples 1 and 2, we saw numerical result of pore size and formation time match well with the exact solution. The exact solution of porosity change can also be derived. Since volume of solid phase is easier to calculate, so we compare the exact solution of solid volume with numerical result. And this time we use the whole region and calculate up to the pore formation time. Take Example 1, when radius $0.15 \leqslant R \leqslant 0.25$, the solid volume is the sum of eight balls' volume; after that and before pore closes off ($0.25 < R \leqslant 0.25\sqrt{2}$), the solid volume is the sum of eight balls' volume deducting the volume of all intersection parts. There are 12 such intersections, each of them has volume

$$2\int\int_{x^2+y^2\leqslant R^2-0.25^2}\left(\sqrt{R^2-(x^2+y^2)}-0.25\right)\mathrm{d}x\,\mathrm{d}y = 2\int_0^{2\pi}\mathrm{d}\theta\int_0^{\sqrt{R^2-0.25^2}}\left(\sqrt{R^2-r^2}-0.25\right)\mathrm{d}r$$
$$= \pi\left(\frac{1}{96}-\frac{1}{2}R^2+\frac{4}{3}R^3\right).$$

Now we have the exact solution for solid volume:

$$V=\begin{cases} 8\times\frac{4}{3}\pi R^3 & 0.15\leqslant R\leqslant 0.25,\\ 8\times\frac{4}{3}\pi R^3-12\pi(\frac{1}{96}-\frac{1}{2}R^2+\frac{4}{3}R^3) & 0.25<R\leqslant 0.25\sqrt{2}. \end{cases} \tag{15}$$

Similarly, for Example 2, with 54 intersections, we have exact solid volume:

$$V=\begin{cases} 27\times\frac{4}{3}\pi R^3 & 0.10\leqslant R\leqslant 0.15,\\ 27\times\frac{4}{3}\pi R^3-54\pi(\frac{9}{4000}-\frac{3}{10}R^2+\frac{4}{3}R^3) & 0.15<R\leqslant 0.15\sqrt{2}. \end{cases} \tag{16}$$

We plot the numerical result of solid volume against the exact solutions in Fig. 8, it shows they match well.

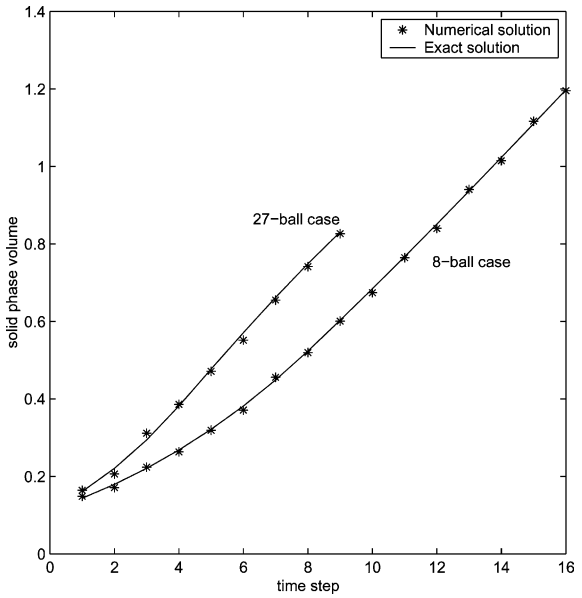


Fig. 8. Solid volume change: numerical vs. exact solution.

**Example 3.** Initially we place 63 balls of the same radius $r = 0.08$ randomly inside the central cube. In order to increase the chance of forming inaccessible pore, all balls are placed at least $2 \times r$ away from the center (see Fig. 9). No exact solution is available for this initial configuration. We can only see the result from numerical solution. The size of inaccessible pore(s) and porosity change is plotted in Fig. 10. Fig. 10(a)

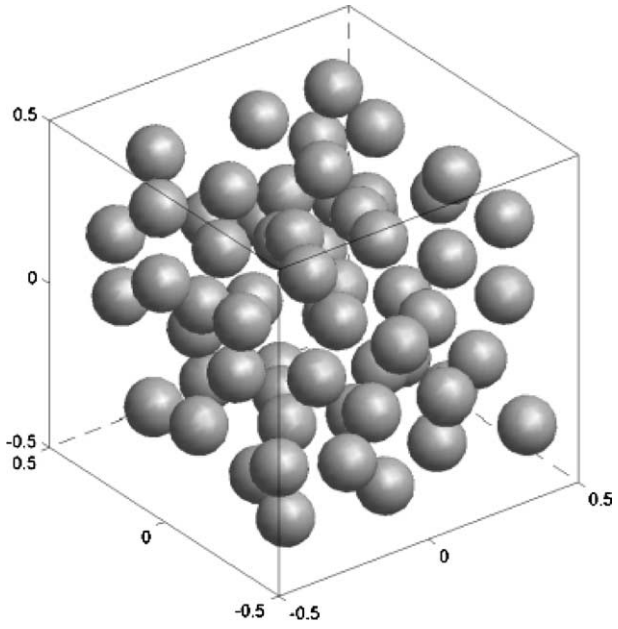


Fig. 9. Initial distribution: 63 balls randomly placed.

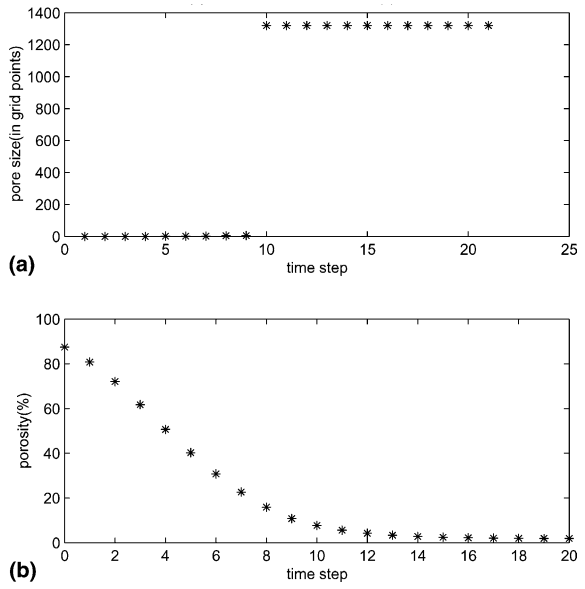


Fig. 10. Pore size and porosity vs time: randomly placed balls. (a) Size of inaccessible pore(s) vs. time. (b) Porosity vs. time.

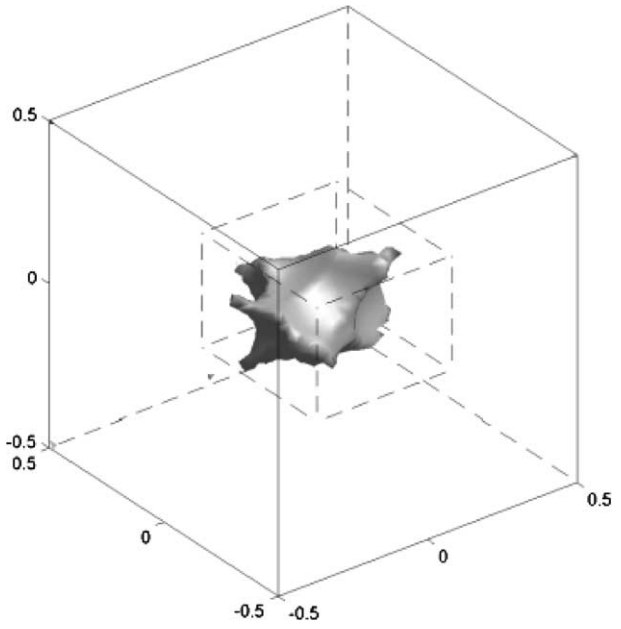


Fig. 11. Inaccessible pore, shape and location: randomly placed balls.

indicates that inaccessible pore(s) form at time $t = 9\Delta t$. Using detecting algorithm for inaccessible pores, we find one pore inside cube $[-0.2, 0.25] \times [-0.275, 0.225] \times [-0.175, 0.175]$. The shape of this pore is shown in Fig. 11.

## 5. Conclusion

In this paper we introduce a phenomenological model and a corresponding numerical methods for the study of pore evolution in three-dimensional CVI process. This method is a natural extension of our previous work on two-dimensional CVI process [13,14]. This method, consisting of a finite difference approximation of the level set equation for fiber front and a Fast Searching Method to detect inaccessible pores, allows the robust computation of the fiber growth and can handle topological change and pore formation at ease. The numerical experiments show that the model can precisely describe the desired growth property of a 3D CVI process in the kinetic limit where the growth speed is a constant. It predicts not only the residual porosity, but also the precise formation time, locations and shapes of all pores.

## References

[1] L. Lehman, S.K. El-Rahaiby, J.B. Wachtman (Eds.), Handbook on Continuous Fiber-reinforced Ceramic Matrix Composites, American Ceramic Society, 1995.
[2] K.S. Mazdiyasni (Ed.), Fiber reinforced ceramic composites: materials, processing, and technology, Noyes Publications, Parkridge, NJ, 1990.
[3] L.C. Evans, Partial Differential Equations, Amer. Math. Soc., Providence, 1998.
[4] J.A. Sethian, Level Set Methods, Cambridge University Press, Cambridge, 1996.
[5] E. Angel, Interactive Computer Graphics a Top-down Approach with OpenGL, second ed., Addison Wesley, Reading, MA, 2000.
[6] H.-C. Chang, D. Gottlieb, M. Marion, B.W. Sheldon, Mathematical analysis and optimization of infiltration process, J. Sci. Comp. 13 (1998) 303–321.

[7] S. Vaidyaraman, W. Lackey, P. Agrawal, T. Starr, 1-D model for forced flow-thermal gradient chemical vapor infiltration process for carbon/carbon composites, Carbon 34 (9) (1996) 1123–1133.
[8] B.W. Sheldon, T.M. Besmann, Reaction and diffusion kinetics during the initial stage of isothermal chemical vapor infiltration, J. Am. Ceram. Soc. 74 (12) (1991) 3046–3052.
[9] D.J. Skamser, D.P. Bentz, R.T. Covrdale, et al., Calculation of the thermal conductivity and gas permeability in a uniaxial bundle of fibers, J. Am. Ceram. Soc. 77 (10) (1994) 2669–2680.
[10] M. Tomadakis, S. Sotirchos, Effective Knudsen diffusivities in structures of randomly overlapping fibers, AIChE J. 37 (1) (1991) 74–86.
[11] M. Tomadakis, S. Sotirchos, Knudsen diffusivities and properties of structures of unidirectional fibers, AIChE J. 37 (8) (1991) 1175–1186.
[12] M. Tomadakis, S. Sotirchos, Transport properties of random arrays of freely overlapping cylinders with various orientation distributions, J. Chem. Phys. 98 (1) (1993) 616–626.
[13] S. Jin, X.L. Wang, T.L. Starr, A model for front evolution with a non-local growth rate, J. Mater. Res. 14 (1999) 3829–3832.
[14] S. Jin, X.L. Wang, T.L. Starr, X.F. Chen, Robust numerical simulation of porosity evolution in chemical vapor infiltration I: two space dimension, J. Comp. Phys. 162 (2000) 467–482.
[15] T.L. Starr, A. Smith, T. Bensmann, J. McLaughlin, B. Sheldon, Modeling of chemical vapor infiltration for composite fabrication, in: 6th European Comference on Composite Materials, Sep. (1993) 231–239.
[16] S. Jin, X.L. Wang, Robust numerical simulation of porosity evolution in chemical vapor infiltration II: anisotropic fronts, J. Comp. Phys. 179 (2002) 57–577.
[17] S. Gupte, J. Tsamopoulos, Densification of porous materials by chemical vapor infiltration, J. Electrochem. Soc. 136 (2) (1989) 555–561.
[18] R. Bickerdike, A. Brown, G. Huges, H. Ranson, in: Proceedings of the Fifth Conference on Carbon, Pergamon press, New York, 1962, pp. 575–582.
[19] S. Osher, J.A. Sethian, Fronts propagating with curvature-dependent speed: algorithms based on Hamilton–Jacobi formulations, J. Comp. Phys. 78 (1988) 12–49.
[20] J. Hoshen, R. Kopelman, Percolation and cluster distribution. I. Cluster multiple labeling technique and critical concentration algorithm, Phys. Rev. B 14 (8) (1976) 15.
[21] S. Sotirchos, S. Zarkanitis, A distributed pore size and length model for porous media reacting with diminishing porosity, Chem. Eng. Sci. 48 (8) (1993) 1487–1502.